Available online at www.sciencedirect.com
ScienceDirect
Icarus 193 (2008) 267–282
ICARUS
www.elsevier.com/locate/icarus

Orbital resonances in the inner neptunian system II. Resonant history of Proteus, Larissa, Galatea, and Despina

Ke Zhang *, Douglas P. Hamilton

Department of Astronomy, University of Maryland, College Park, MD 20742, USA

Received 18 March 2007; revised 8 August 2007

Available online 14 September 2007

Abstract

We investigate the orbital history of the small neptunian satellites discovered by *Voyager 2*. Over the age of the Solar System, tidal forces have caused the satellites to migrate radially, bringing them through mean-motion resonances with one another. In this paper, we extend our study of the largest satellites Proteus and Larissa [Zhang, K., Hamilton, D.P., 2007. Icarus 188, 386–399] by adding in mid-sized Galatea and Despina. We test the hypothesis that these moons all formed with zero inclinations, and that orbital resonances excited their tilts during tidal migration. We find that the current orbital inclinations of Proteus, Galatea, and Despina are consistent with resonant excitation if they have a common density $0.4 < \bar{\rho} < 0.8$ g/cm^3. Larissa's inclination, however, is too large to have been caused by resonant kicks between these four satellites; we suggest that a prior resonant capture event involving either Naiad or Thalassa is responsible. Our solution requires at least three past resonances with Proteus, which helps constrain the tidal migration timescale and thus Neptune's tidal quality factor: $9000 < Q_N < 36{,}000$. We also improve our determination of Q_s for Proteus and Larissa, finding $36 < Q_P < 700$ and $18 < Q_L < 200$. Finally, we derive a more general resonant capture condition, and work out a resonant overlap criterion relevant to satellite orbital evolution around an oblate primary.
Published by Elsevier Inc.

Keywords: Resonances, orbital; Neptune, satellites; Triton; Satellites, dynamics

1. Introduction

Voyager 2 discovered six small satellites (Table 1) around Neptune in 1989 (Smith et al., 1989). These satellites likely formed after the capture of the planet's largest moon, Triton (McKinnon, 1984; Goldreich et al., 1989; Agnor and Hamilton, 2006). Triton's capture and subsequent orbital migration and circularization (McCord, 1966) destroyed the original moon system and formed a debris disk, which was both scattered away and swept up by the giant moon (Ćuk and Gladman, 2005). Only debris close to Neptune survived this catastrophe, and resonant encounters with Triton kept a new generation of satellites from forming in this inner disk until Triton finished evolving to its current circular orbit (Hamilton et al., 2005). The post-captured orbital circularization occurred initially on a timescale of a hundred thousand years due to physical interactions with the debris disk (Ćuk and Gladman, 2005), and then on a longer timescale of a hundred million years due to tides (Goldreich and Soter, 1966). Thus all six of Neptune's inner moonlets most likely formed after Triton attained its current circular, retrograde, and highly-inclined orbit.

Today, Triton's large orbital tilt induces a strong forced component in the inclination of each satellite's orbit. These forced inclinations define the location of the warped Laplacian plane, about whose normal satellites' orbital planes precess (Zhang and Hamilton, 2007). Measured from their local Laplace planes, the current free orbital inclinations ($i^{\rm fr}$) of the small satellites are only a few hundredths to tenths of a degree, with one exception (4.75° for tiny Naiad). It is the contention of this paper, and a result of our previous study in Zhang and Hamilton (2007), that these free tilts, despite being very small, arose from resonant excitations during orbital evolution. Physically, the debris disk from which the satellites formed should have damped rapidly into a very thin layer lying in the warped Laplacian plane. Satellites formed from this slim disk should initially have free inclinations $i^{\rm fr} \ll 0.001°$, perhaps similar to

* Corresponding author. Fax: +1 (831) 459 3074.
E-mail address: kzh@pmc.ucsc.edu (K. Zhang).

0019-1035/$ – see front matter Published by Elsevier Inc.
doi:10.1016/j.icarus.2007.08.024

Table 1
Inner neptunian satellites and Triton

Name	$\bar{R}$ (km)	a (km)	e ($\times 10^{-3}$)	$i^{\rm Lap}$ (°)	$i^{\rm fr}$ (°)
Naiad	33 ± 3	48,227	0.4 ± 0.3	0.5118	4.75 ± 0.03
Thalassa	41 ± 3	50,075	0.2 ± 0.2	0.5130	0.21 ± 0.02
Despina	75 ± 3	52,526	0.2 ± 0.2	0.5149	0.06 ± 0.01
Galatea	88 ± 4	61,953	0.04 ± 0.09	0.5262	0.06 ± 0.01
Larissa	97 ± 3	73,548	1.39 ± 0.08	0.5545	0.205 ± 0.009
Proteus	210 ± 7	117,647	0.53 ± 0.09	1.0546	0.026 ± 0.007
Triton	1353	354,759	0.0157	–	156.83[a]

Radii of the small satellites ($\bar{R}$) are from Karkoschka (2003); moonlet orbital elements (semi-major axis a, eccentricity e, inclination of local Laplacian plane $i^{\rm Lap}$, and free inclination $i^{\rm fr}$) are from Jacobson and Owen (2004); Triton parameters are from Jacobson et al. (1991).

[a] Inclination of Triton is relative to the invariable plane.

the current thickness of Saturn's ring ($i \sim 0.0001°$). Collisions amongst ring particles damp orbital energy while preserving angular momentum, leading inexorably to tiny tilts. Unless large moons have unrealistic scattering histories in the late stages of satellite accretion, the newly-formed satellites inherit the near-zero tilt of the parent disk. A reasonable explanation for the current non-zero inclinations of the satellites thus requires an examination of their orbital evolution history.

Planetary tides cause orbital evolution of the small neptunian satellites and have brought them into and out of resonant configurations. In our previous paper (Zhang and Hamilton, 2007), we examined the recent strong 2:1 mean-motion resonance passage between Proteus and Larissa (abbreviated *PL 2:1*) which occurred only a few hundred million years ago. During the resonance, Larissa completes two orbits for every one that Proteus does and rapid orbital evolution can occur. We carried out extensive numerical simulations for this resonance passage, and identified a new type of three-body resonance between the satellite pair and Triton. In order to study these resonances analytically, we generalized the definition of orbital elements in the inner neptunian system to incorporate the secular effects of Triton: free inclinations are measured relative to a satellite's local Laplace plane ($i^{\rm fr}$), and longitudes are all "bent" angles measured partially in this plane ($\tilde{\Omega}$ and $\tilde{\varpi}$, see Fig. 5 of Zhang and Hamilton, 2007).

Mean-motion resonances are characterized by a resonant argument or resonant angle ϕ. When two or more satellites are exactly in resonance, $\dot{\phi} = 0$. In the inner neptunian system, the strongest resonant arguments have the form

$$\phi = (p+q)\lambda_2 - p\lambda_1 + j_1\tilde{\varpi}_1 + j_2\tilde{\varpi}_2 + j_3\tilde{\Omega}_1 + j_4\tilde{\Omega}_2 + j_T\Omega_T. \quad (1)$$

This is the standard argument for a two-body resonance augmented by an extra term $j_T\Omega_T$ to include Triton's effect (Zhang and Hamilton, 2007). Here λ_1 and λ_2 are the orbital mean longitudes of the inner and outer small satellites, respectively, which vary rapidly in time. The node and pericenter angles ($\tilde{\Omega}_1$, $\tilde{\Omega}_2$ and $\tilde{\varpi}_1$, $\tilde{\varpi}_2$) are longitudes defined by Zhang and Hamilton (2007); these only change slowly and Ω_T, the longitude of the ascending node of Triton, varies even more slowly. The numerical coefficients in front of the longitudes ($p > 0$, $q > 0$, and j_i) are all integers and are subject to additional constraints discussed by Hamilton (1994).

Three-body resonances are usually weaker than their two-body counterparts because their resonant strengths contain an extra small term proportional to the mass ratio of the third body and the primary. In the Neptune–Triton system, however, three-body inclination resonances are stronger than their two-body counterparts due to Triton's large tilt. With the help of the three-body resonant kicks, typical inclination excitations of Proteus and Larissa are smaller than, but roughly the same magnitude as, the satellites' current free inclinations (Zhang and Hamilton, 2007). In particular, if the two satellites had a large common mean density $\bar{\rho} > 1.5$ g/cm^3, Proteus could acquire its current tilt through the *PL 2:1* resonance passage alone. The inclination of Larissa, on the other hand, could be excited to only about half its current value. We concluded that additional resonance passages were necessary.

An additional density constraint arises from the current non-zero eccentricities of the satellites (Table 1). Without a recent excitation, these eccentricities should have damped to zero due to satellite tides acting over billions of years (Burns, 1977). The recent *PL 2:1* resonance, however, excited eccentricities to larger than today's values if the satellite masses are large enough, leading to the constraint $\bar{\rho} > 0.05$ g/cm^3.

In the present paper, we investigate earlier resonance passages among the four largest inner neptunian moons: Proteus, Larissa, Galatea, and Despina, with the goals of (i) solving the mystery of Larissa's inclination excess, (ii) finding a consistent excitation scenario for the orbital tilts of all four satellites, and (iii) constraining satellite densities and Neptune's tidal Q. For now, we ignore the innermost Naiad and Thalassa whose masses are ~10 times smaller than those of the other moons (Table 1). In next section, we study the tidal migration history of the four satellites and enumerate the possible resonance passages among them. We then detail our numerical simulations of the most important resonances and their immediate implications. Finally, we combine the results of multiple resonance passages to place much stronger constraints on satellite densities, as well as Q_N, Q_P, and Q_L, than we could using Proteus and Larissa alone (Zhang and Hamilton, 2007).

2. Resonant history of the neptunian system

The long-term evolution of satellite orbits is determined by tidal dissipation within the parent planet (Burns, 1977). A small satellite raises tides on Neptune (planetary tides), which then act back on the satellite gravitationally and causes it to migrate radially at a rate

$$\frac{\dot{a}}{a} = \pm\frac{3k_{2N}}{Q_N}\left(\frac{R_N}{a}\right)^5 \mu n \quad (2)$$

(Murray and Dermott, 1999, Section 4.9). Here a, and n are the semi-major axis and mean motion of the satellite, respectively, and μ is the satellite–planet mass ratio. The Love number k_{2N} measures the internal rigidity of Neptune, and Q_N is its tidal dissipation factor which parameterizes the energy loss due to

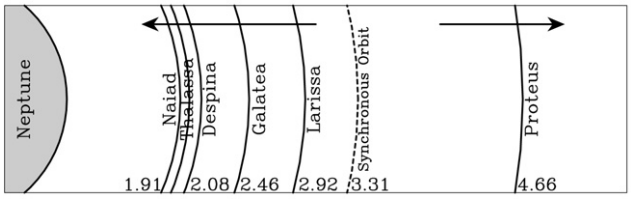

Fig. 1. Semi-major axes of the small inner neptunian satellites in planet radii. The two arrows indicate the direction of tidal migration.

tides. Both k_{2N} and Q_N are poorly constrained observationally. The former, however, is less dependent on the planet's internal structure, so in this paper, we adopt the theoretically-determined $k_{2N} = 0.41$ (Burša, 1992) and constrain Q_N. The sign of the right-hand side of Eq. (2) depends on which side of synchronous orbit, the location where a satellite orbits at the same angular rate as Neptune rotates, the satellite is located. If a prograde satellite is outside synchronous orbit, it orbits slower than Neptune rotates and tides push it outwards ($\dot{a} > 0$); otherwise, tides pull it inward towards Neptune ($\dot{a} < 0$). The synchronous orbit lies at $3.31R_N$, between the orbits of Proteus and Larissa (Fig. 1). Hence, Proteus migrates away from Neptune, while all other satellites spiral inwards, which is likely the origin of the large gap between the orbits of Proteus and Larissa. A satellite's migration rate is proportional to its mass, and has a steep inverse dependence on its orbital semi-major axis (Eq. (2)). Since Larissa, Galatea, and Despina have comparable masses (within a factor of 2), the innermost of these migrates most rapidly, and hence their orbits all diverge from one another. Diverging orbits usually lead to resonant kicks during which satellite orbital elements change sharply (Hamilton and Burns, 1993; Zhang and Hamilton, 2007). Due to the much smaller masses of the innermost Naiad and Thalassa, their orbits evolve more slowly and are approached by those of the next three satellites. Converging orbits typically lead to resonant trapping, as has been suggested as the explanation for the large inclination of Naiad by Banfield and Murray (1992).

Not only do satellites raise tides on Neptune (planetary tides), but the planet raises tides on satellites as well (satellite tides). Satellite tides circularize orbits of the neptunian satellites on timescales of several hundred million years. Importantly, neither planetary nor satellite tides affect satellite orbital inclinations significantly (Burns, 1977). The rotation of the planet can cause its tidal bulge to shift slightly out of the satellite's orbital plane, but the resulting force components perpendicular to the orbital plane are weak, and can only cause very slow inclination evolution. In principal, non-zero satellite obliquities (so-called Cassini states; Colombo, 1966; Hamilton and Ward, 2004; Ward and Hamilton, 2004) might allow satellite tides to damp inclinations. But the current observed satellite inclinations, measured in radians, are about 10 times larger than eccentricities (Table 1), thus the inclination damping rate must be substantially smaller than the eccentricity damping rate. Tides have most likely changed the inclinations of the inner neptunian satellites by less than a tenth of their current values in the past 4 billion years.

As satellites migrate, changes of their mean motions bring them into and out of resonances (Greenberg, 1973), which kick up their orbital eccentricities and inclinations. Resonance-excited eccentricities damp away quickly due to satellite tides (Goldreich, 1963), but without an effective damping mechanism, any inclination acquired is retained essentially permanently.

Over the history of the Solar System, the inner neptunian satellites have migrated on the order of R_N (Fig. 1), which is slow enough that most of the first- and second-order mean-motion resonances are traversed in the adiabatic limit. Magnitudes of resonant kicks on satellite inclinations are then predictable both analytically (Peale, 1976) and numerically (Zhang and Hamilton, 2007). Higher-order resonances are often not transversed adiabatically, but we have found that their kicks are typically smaller by about an order of magnitude, and thus add negligibly to the total inclination growth of the moons.

Because satellite mean motions are much larger than orbital precession rates, resonances cluster in discrete narrow zones near where the ratio of satellite orbital periods is a rational number ($(p+q)/p$, see Zhang and Hamilton, 2007). We integrate Eq. (2) for each satellite and locate all the first- and second-order resonant zones ($q = 1$ and $q = 2$ in Eq. (1)), as shown in Fig. 2. We stop the integration when Larissa is fairly close to the synchronous orbit and the unphysical discontinuity in $\dot{a}/a$ (Eq. (2)) becomes problematic. Because of this over-simplification for satellites near synchronous orbit, the left-hand side of the plot is less accurate than the right, especially for Larissa. As the time axis indicates, the integration is much longer than the age of the Solar System, but the evolutionary timescale depends on Neptune's Q and the satellite masses, all of which are poorly constrained. Here we have used $Q_N = 20{,}000$ and a common satellite mean density $\bar{\rho} = 0.6$ g/cm^3. For these assumptions, Proteus was $0.28R_N$ closer to Neptune 4 billion years ago than it is today and Larissa, Galatea, and Despina have each migrated towards the planet by 0.24, 0.39, and $0.49R_N$, respectively. A larger Q_N or a lower satellite density would result in a slower evolution, as described in Fig. 2's caption. Thus the origin of the system could occur anywhere along the horizontal axis of Fig. 2, depending on the actual values of Q_N and $\bar{\rho}$.

With our assumptions of $Q_N = 20{,}000$ and $\bar{\rho} = 0.6$ g/cm^3, the satellites go through approximately 16 resonant zones involving first- and second-order mean-motion resonances (Fig. 2) since the system formed ~4 billion years ago (Hamilton et al., 2005). For different Q_N and $\bar{\rho}$, a different number of past resonances would have occurred. Our strategy here is to work backwards in time from the present to find out which of these resonances actually occurred and determine what their effects were. We focus on orbital inclinations which are relatively unaffected by tides and hence accumulate over time, leaving an orbital "fossil record" still visible today.

3. Resonances with Proteus

In Zhang and Hamilton (2007), we found that the magnitudes of resonant kicks on orbital inclinations depended

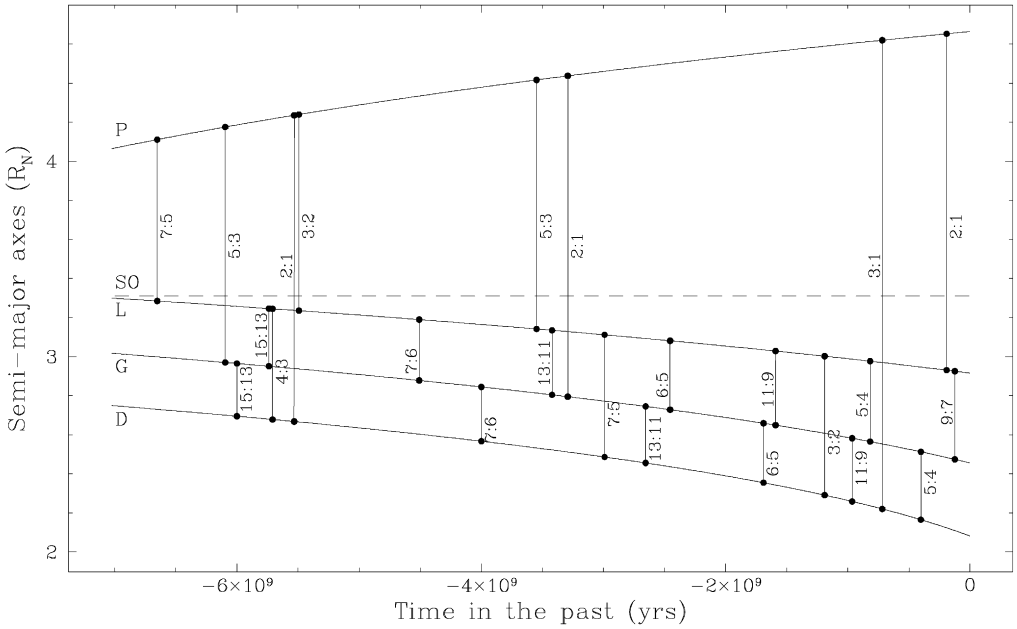

Fig. 2. Possible past first- and second-order mean-motion resonances between satellite pairs Proteus (P), Larissa (L), Galatea (G), and Despina (D). We integrate Eq. (2) backward in time until Larissa is fairly close to the synchronous orbit (SO), assuming $Q_N = 20{,}000$ and a uniform satellite mean density of $\bar{\rho} = 0.6\ \mathrm{g/cm^3}$. Black solid curves show the migration tracks of the four satellites, and the dashed horizontal line denotes the synchronous orbit. The vertical lines represent strong resonant zones for different pairs of satellites. The time scale along the bottom axis depends on both Q_N and $\bar{\rho}$. For different values of these parameters, simply multiply all times by the factor $\frac{Q_N/20{,}000}{\bar{\rho}/(0.6\ \mathrm{g/cm^3})}$.

strongly on the mass of the perturber. Since Proteus is by far the largest satellite near Neptune, resonances between it and the other satellites are much stronger than those among the three smaller satellites. As a first approximation, therefore, we examine only the Proteus resonances, neglect the weaker ones, and see if we can form a consistent story from this subset of Fig. 2. We will return to consider resonances between Larissa, Galatea, and Despina in Section 4.2. In addition to the very recent 2:1 resonant zone between Proteus and Larissa, Proteus might have gone through seven other resonant zones that we list backwards from the present: *PD 3:1*, *PG 2:1*, *PL 5:3*, *PL 3:2*, *PD 2:1*, *PG 5:3*, and *PL 7:5*. In this section, we detail these resonance passages, determine the inclination excitation provided by each resonance, and analyze new features found in our simulations.

The most straight-forward numerical study would simply integrate the whole 4 billion years history of the neptunian system directly. This is, however, impractical due to current computational limits. Since the most important orbital evolution occurs during resonance passages which occupy only a relatively short period of time (<20 Myrs), we use the HNDrag package to integrate just the passage of each resonant zone directly. We then solve the tidal migration equations for the intervening times. Each simulation includes Neptune, Triton, and the two relevant satellites. In practice, we start with zero free eccentricity and free inclination for both orbits prior to each resonance passage, and correct for the effects of inclinations from earlier resonance passages using the technique discussed in Section 4.

3.1. The most recent PL 2:1 resonance

This most recent resonant zone is located merely several hundred kilometers away from the current orbits of Proteus and Larissa. Based on our simple tidal model, the resonance occurred only a few hundred million years ago. We studied this resonance passage in great detail in Zhang and Hamilton (2007), and found that not only did it excite the moons' orbital tilts, but it also can explain the larger than average eccentricities of their orbits—the excitation is too recent for the eccentricities to have fully damped away. Fig. 3 is similar to Fig. 2 of Zhang and Hamilton (2007), but with different assumed $\bar{\rho}$ and Q_N. The plot shows the eccentricities and free inclinations of Proteus and Larissa when they pass through the resonant zone. Three-body resonances dominate the inclination evolution; the investigations presented below show that these special resonances are common in the Neptune–Triton system.

3.2. The second-order resonance PD 3:1

The previous resonant zone Proteus traversed consists of the 3:1 resonances with Despina (cf. Fig. 2). The 3:1 resonant zone is simpler than the 2:1 one as it contains only second-order, fourth-order, and other even-order resonances. Compared to the *PL 2:1* zone (Fig. 3), which has first-order eccentricity resonances, there are no strong eccentricity kicks, and the lack of third-order resonances makes the inclination evolution much simpler and cleaner as well (Fig. 4). The two second-order three-body resonant kicks, $R_{i_P i_T}$ and $R_{i_L i_T}$, dominate the inclination growth. Two of the three traditional second-order two-body resonances can be easily identified, and fourth- and

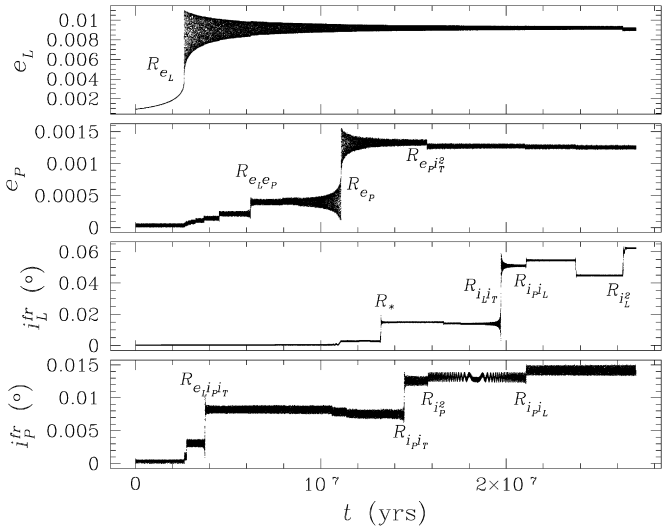

Fig. 3. The eccentricities and free inclinations of Proteus and Larissa as they diverge through the *PL 2:1* resonances. The system consists of Neptune, Triton, and the two small satellites, started with zero free eccentricities and free inclinations. The proximity of the strong first-order R_{e_L} resonance forces $e_L \approx 0.001$ at $t = 0$; starting close to resonance with this value is equivalent to starting with $e_L = 0$ at a greater distance from the resonance as actually occurs in the system. The density of the satellites is $\bar{\rho} = 0.6$ g/cm^3; a_L is fixed at $2.93R_N$, while Proteus migrates outward from $4.651R_N$ to $4.654R_N$, equivalent to $Q_N = 20{,}000$. The strongest first-, second-, and third-order resonances are identified using the notation of Zhang and Hamilton (2007) (e.g., $R_{i_P i_L}$ is a second-order resonance involving the inclinations of Proteus and Larissa). Second-order ($R_{i_P i_T}$, and $R_{i_L i_T}$) and third-order ($R_{e_L i_P i_T}$ and R_*) three-body resonances dominate the inclination growth; these resonances are discussed in detail in Zhang and Hamilton (2007). Unlabeled-kicks are due to weaker higher-order resonances.

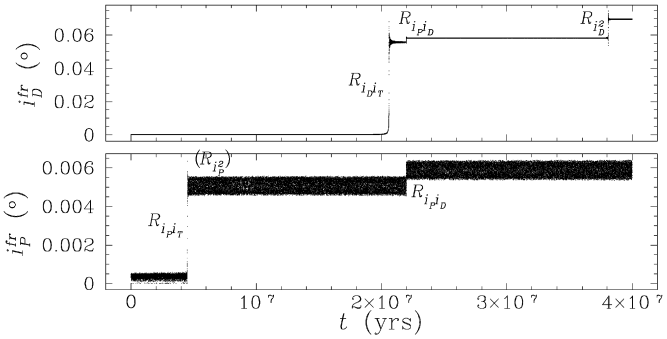

Fig. 4. Proteus and Despina diverge through the *PD 3:1* resonant zone. The mean satellite density is $\bar{\rho} = 0.8$ g/cm^3, and $Q_N = 33{,}000$. Both satellites are initially on circular orbits in their local Laplace planes. Two of the three usual second-order resonances are identified ($R_{i_P i_D}$ and $R_{i_D^2}$), as well as the two three-body resonances, $R_{i_P i_T}$ and $R_{i_D i_T}$. Note that although the effects of the third second-order resonance ($R_{i_P^2}$) are too weak to be visible, we indicate its approximate location.

higher-order kicks are too weak to have noticeable effects. The overall *PD 3:1* inclination kick on Despina is a little smaller than the overall *PL 2:1* kick on Larissa, and the Proteus kick through the *PD 3:1* is weaker by a factor of 3 due both to the smaller mass of Despina ($m_D \approx 0.5 m_L$) and to the lack of contributions from odd-order resonances. In Zhang and Hamilton (2007), we pointed out that strong third-order three-body resonances contributed significantly to the growth of $i_P^{\rm fr}$ ($R_{e_L i_P i_T}$ and R_* in Fig. 3). These resonances do not exist in the *PL 3:1* and other second-order resonant zones, including the *PL 5:3*, *PG 5:3* and *PL 7:5* from Fig. 2.

3.3. The PG 2:1 and diverging capture

The 2:1 resonant zone between Proteus and Galatea is located between *PD 3:1* and *PL 5:3*. This resonance is similar to the first-order *PL 2:1* discussed above, with differences arising only from the smaller mass ratio of the two satellites and their different distances from Neptune. The two first-order eccentricity resonances (R_{e_G} and R_{e_P}) kick the orbital eccentricities of the two satellites strongly, as can be seen in Fig. 5. The inclination kicks due to three-body resonances ($R_{i_P i_T}$, $R_{i_G i_T}$, $R_{e_G i_P i_T}$, and R_*) are similar in magnitude to those due to the *PL 2:1* resonances discussed in Section 3.1. In a small fraction of our simulations, such as the one shown in Fig. 5, however, we see a new effect that is surprising at first glance: resonance capture.

In addition to resonant kicks, when satellite orbits are subject to sudden and sharp changes, two satellites may also be captured into a mean-motion resonance during tidal migration (Greenberg, 1977). When this occurs, the mean motions and orbital precession rates of the two satellites vary in such a way that the associated resonant angle librates around a stationary point rather than cycling through a full 360°. The affected eccentricity or inclination grows until nearby resonances or other perturbations break the system out of resonance. What is surprising here is that previous studies have shown that resonant captures during tidal migration occur when the orbits of two satellites approach each other (e.g., Hamilton, 1994), while our satellites are diverging. Earlier papers, however, all focus on strong first- and second-order resonances. For some higher-order resonances, temporary capture is possible for diverging orbits. We have found several such resonant trappings in our simulations when the two orbits diverge slowly enough. Nevertheless, trappings are still very rare even at slow migration rates, probably because of the inherent weakness of higher-order resonances. We have run 10 simulations through the *PG 2:1* zone with $25{,}000 < \frac{Q_N}{\bar{\rho}/(\mathrm{g/cm^3})} < 35{,}000$ for different satellite densities ranging between 0.4 and 1.5 g/cm^3, but there is only one capture event at $\bar{\rho} = 0.8$ g/cm^3, shown in Fig. 5. In this simulation, after the system has gone through the two first-order eccentricity resonances (R_{e_G} and R_{e_P}), the two third-order three-body resonances ($R_{e_G i_P i_T}$ and R_*), and the first second-order three-body resonance ($R_{i_P i_T}$), the two orbits are captured into a three-body resonance $R_{e_P i_T^2}$, second-order in the small quantities e_P and μ_T, with a critical argument

$$\phi_{e_P i_T^2} = 2\lambda_P - \lambda_G + \tilde{\varpi}_P - 2\Omega_T. \tag{3}$$

3.3.1. Resonant trapping condition

We now derive the condition in which resonant trapping into $R_{e_P i_T^2}$ is possible. We assume that away from resonance, tides force Proteus and Galatea to migrate at rates $\dot{a}_P^d$ and $\dot{a}_G^d$, respectively, and that Triton's orbit is fixed in space. Following

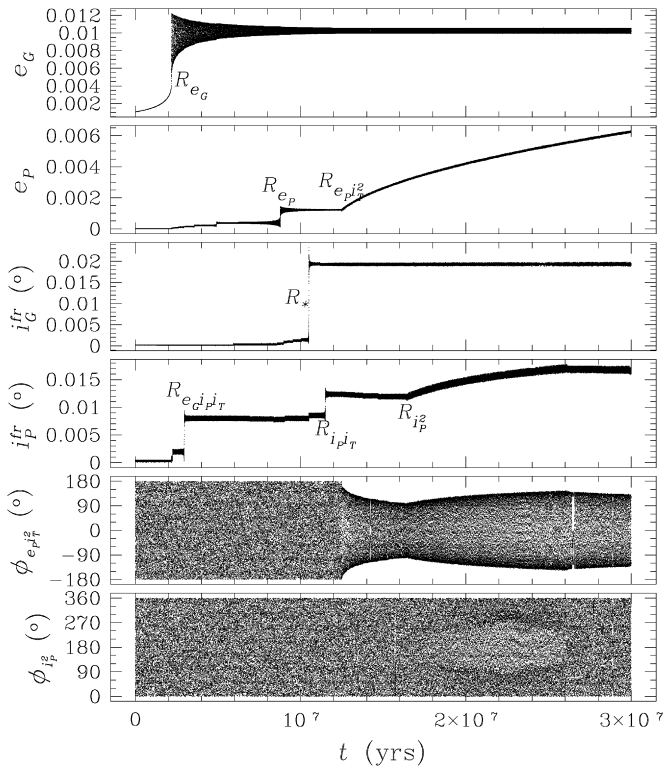

Fig. 5. The *PG 2:1* passage with an isolated eccentricity-type resonance capture; we show eccentricities, free inclinations and the two relevant resonant argument. As in Fig. 3. the initial $e_G \neq 0$ is forced by the strong nearby R_{e_G} resonance. After trapping into the $R_{e_P i_T^2}$ resonance at $t \approx 1.2 \times 10^7$ yrs, Proteus is captured into the second-order resonance ($R_{i_P^2}$) at $t \approx 1.6 \times 10^7$ yrs which affects its inclination. The second capture is enabled by extremely slow changes to $\dot{\tilde{\varpi}}_P$ and $\dot{\tilde{\Omega}}_P$ induced by the first resonance. In this simulation, $\bar{\rho} = 0.8$ g/cm^3 and $Q_N = 22{,}000$.

Hamilton (1994), we derive the rates of change of a_P, a_G, e_P, and i_T due to resonant and tidal perturbations to the lowest order in e and i:

$$\dot{a}_P = \dot{a}_P^d - \frac{4\mu_G \mu_T \beta e_P i_T^2}{n_P a_P} \sin\phi_{e_P i_T^2}, \tag{4}$$

$$\dot{a}_G = \dot{a}_G^d + \frac{2\mu_P \mu_T \beta e_P i_T^2}{n_G a_G} \sin\phi_{e_P i_T^2}, \tag{5}$$

$$\dot{e}_P = \frac{\mu_G \mu_T \beta i_T^2}{n_P a_P^2} \sin\phi_{e_P i_T^2}, \tag{6}$$

$$\dot{i}_T = -\frac{2\mu_G \mu_P \beta e_P i_T}{n_T a_T^2} \sin\phi_{e_P i_T^2}. \tag{7}$$

Here $\beta < 0$ is the resonant strength of $R_{e_P i_T^2}$. In general, β is negative for odd q in the resonant argument equation (1) and positive for even ones. It has the same units as $n^2 a^2$ and its value depends only on satellite semi-major axes. When the two orbits are in any of the 2:1 resonances, their semi-major axes must follow

$$\frac{a_P}{a_G} = \frac{\dot{a}_P}{\dot{a}_G} \approx 2^{2/3}. \tag{8}$$

With Eqs. (4) and (5), and Eq. (8), we can solve for $\sin\phi_{e_P i_T^2}$ at resonant equilibrium:

$$\sin\phi_{e_P i_T^2} = \frac{n_P a_P^2}{2\mu_G \mu_T \beta e_P i_T^2} \frac{\dot{a}_P^d/a_P - \dot{a}_G^d/a_G}{2 + \sqrt[3]{2}\mu_P/\mu_G}. \tag{9}$$

For $\dot{a}_P^d/a_P = \dot{a}_G^d/a_G$, the two equilibrium points are at $\phi_{e_P i_T^2} = 0$ and $\phi_{e_P i_T^2} = 180°$; they are shifted slightly when dissipation is present and the two orbits migrate at different relative rates.

Substituting Eq. (9) into Eq. (6), we obtain

$$2 e_P \dot{e}_P = \frac{\dot{a}_P^d/a_P - \dot{a}_G^d/a_G}{2 + \sqrt[3]{2}\mu_P/\mu_G},$$

which has the solution

$$e_P = \left[e_{P0}^2 + \frac{\dot{a}_P^d/a_P - \dot{a}_G^d/a_G}{2 + \sqrt[3]{2}\mu_P/\mu_G} t \right]^{1/2}, \tag{10}$$

where t is the time elapsed since entering the resonance and e_{P0} is the initial eccentricity of Proteus. If resonant trapping occurs for a low eccentricity, e_P must increase with time and Eq. (10) thus requires

$$\frac{\dot{a}_P^d}{a_P} - \frac{\dot{a}_G^d}{a_G} > 0,$$

or that the two orbits diverge from each other. Note that this is opposite the usual requirement that the orbits converge for trapping to be possible, yet consistent with the behavior of Fig. 5. This interesting result—trapping for diverging orbits—is a direct consequence of the sign of the $\tilde{\varpi}$ term in the resonant angle (Eq. (3)), as we shall see below.

The resonance $R_{e_P i_T^2}$ affects not only the eccentricity of Proteus, but also the inclination of Triton. We can solve for the evolution of i_T with Eqs. (7) and (9):

$$i_T = \left[i_{T0}^2 - \frac{2\mu_P}{\mu_T} \sqrt{\frac{a_P}{a_T}} \left(\frac{\dot{a}_P^d/a_P - \dot{a}_G^d/a_G}{2 + \sqrt[3]{2}\mu_P/\mu_G} \right) \right]^{1/2}, \tag{11}$$

where the second term on the right-hand side is negative for trapping. Thus, if resonant trapping occurs, e_P increases with time while i_T decreases. In typical cases when the satellites have comparable masses, the trapping would cease when i_T drops to zero. Because of Triton's huge mass, however, the change of i_T is negligible compared to that of e_P:

$$\frac{\Delta i_T/i_T}{\Delta e_P/e_P} \sim -\frac{2\mu_P}{\mu_T} \sqrt{\frac{a_P}{a_T}} \approx -0.002.$$

Hence, Triton's inclination decreases ~500 times more slowly than Proteus' eccentricity increases and the resonance trapping can be stable for a long time.

The resonant trapping condition can be easily generalized for an arbitrary resonance with an argument defined by Eq. (1). Following similar procedures, we find that, in order for any relevant eccentricity or inclination to increase, the integer in front of the corresponding node or pericenter angle in Eq. (1), j_i, must obey

$$j_i \left(\frac{\dot{a}_2^d}{a_2} - \frac{\dot{a}_1^d}{a_1} \right) > 0. \tag{12}$$

For standard first-order ($q = 1$) and second-order ($q = 2$) two-body resonances, j_i must be negative, and thus we recover the standard result: resonant trapping is possible only if $\dot{a}_2^d/a_2 - \dot{a}_1^d/a_1 < 0$, i.e., for converging orbits. But for resonances with three or more node and pericenter angles involved, like $R_{e_P i_T^2}$ shown in Eq. (3), some of the j_i can be positive, which makes capture into these resonances possible only for diverging orbits, as we have seen in Fig. 5. Thus it is a general result that, for any isolated mean-motion resonance, capture for converging orbits requires a negative node or pericenter coefficient, while for capture from diverging orbits a positive coefficient is needed.

3.3.2. Evolution in $R_{e_P i_T^2}$

We now look at the resonant angle during the resonant trapping (the fifth panel of Fig. 5). Assuming moderate eccentricities so that the pericenter term in Eq. (3) is negligible, $\phi_{e_P i_T^2}$ satisfies

$$\ddot{\phi}_{e_P i_T^2} = 2\dot{n}_P - \dot{n}_G,$$

which can be easily transformed into a harmonic equation using Eqs. (4) and (5):

$$\ddot{\phi}_{e_P i_T^2} + \omega_0^2 \sin\phi_{e_P i_T^2} + \left(\dot{n}_G^d - 2\dot{n}_P^d\right) = 0, \tag{13}$$

where $\dot{n}_P^d = -(3/2) n_P \dot{a}_P^d/a_P$ and $\dot{n}_G^d = -(3/2) n_G \dot{a}_G^d/a_G$ are the tidal drag rates of the two orbits expressed in terms of mean motions. Equation (13) is a standard harmonic oscillator with small-angle libration frequency ω_0 given by

$$\omega_0^2 = -\frac{6\mu_T \beta e_P i_T^2}{a_P^2}\left(2\mu_G + \sqrt[3]{2}\mu_P\right).$$

As shown in Fig. 5, $\phi_{e_P i_T^2}$ begins to librate around a stable equilibrium point at 0° as the orbits are first trapped into the $R_{e_P i_T^2}$ resonance. In fact, the divergence forced by tidal dissipation causes the equilibrium point to shift to a small negative value determined by Eq. (9). Averaging over a libration, Eqs. (4) and (5) simplify to

$$\dot{a}_P = \dot{a}_P^d - \delta_P,$$
$$\dot{a}_G = \dot{a}_G^d + \delta_G,$$

where δ_P and δ_G are small positive quantities. These terms resist the tidal divergence and allow the approximate resonance condition (Eq. (8)) to be maintained.

For slow changes of ω_0, the system has an adiabatic invariant (Landau and Lifshitz, 1976, Section 49)

$$\omega_0 \Phi^2 = \text{constant},$$

where Φ (assumed small) is the libration width, or the amplitude of the oscillating resonant angle $\phi_{e_P i_T^2}$. As e_P increases slowly, ω_0 grows and Φ decreases as shown in Fig. 5 from 1.2×10^7 years until 1.6×10^7 years when a second resonance is activated.

3.3.3. Trapping into $R_{i_P^2}$

Shortly after capture into $R_{e_P i_T^2}$, the two satellites are trapped into the traditional two-body resonance $R_{i_P^2}$ (Fig. 5), with a resonant argument

$$\phi_{i_P^2} = 4\lambda_P - 2\lambda_G - 2\tilde{\Omega}_P.$$

The interplay between the two active resonances is quite interesting. With both resonances active, the orbits still appear to diverge, as can be seen from Eq. (10) and the fact that e_P continues to rise in Fig. 5. But, coincident with the second capture, there is an abrupt change in the behavior of $\phi_{e_P i_T^2}$ (fifth panel of Fig. 5) whose libration changes from decreasing with time (as expected for an isolated resonance) to increasing with time. This state of affairs continues until $t = 2.6 \times 10^7$ years at which point the second resonance ceases to be active (note the flattening of the i_P curve) and the libration amplitude of $\phi_{e_P i_T^2}$ begins decreasing again.

The sharp-eyed reader might have noticed a very subtle change in the density of points for the $\phi_{i_P^2}$ history (sixth panel of Fig. 5)—an oval-shaped feature between $t = 1.6 \times 10^7$ and 2.6×10^7 years that indicates that the $R_{i_P^2}$ resonance is active. The oval feature has dark edges (turning points—note the similar dark edges in the fifth panel) and a lighter center because the system spends more time near $\phi_{i_P^2} = 0$ than near $\phi_{i_P^2} = 180°$. The $R_{i_P^2}$ resonance is prevented from cleanly librating about $\phi_{i_P^2} = 0$ by the more powerful $R_{e_P i_T^2}$ resonance, but the asymmetry in the density of points that it produces is enough to cause the systematic rise in Proteus' free inclination (Fig. 5, fourth panel). The libration of the resonant angle $\phi_{i_P^2}$ initially decreases (from 1.6×10^7 yr $< t < 2.2 \times 10^7$ yr) and then increases again (from 2.2×10^7 yr $< t < 2.6 \times 10^7$ yr) until the orbits finally exit the $R_{i_P^2}$ resonance.

The $R_{i_P^2}$ resonance usually requires converging orbits to trap into the stable equilibrium point $\phi_{i_P^2} \approx 180°$ (Murray and Dermott, 1999). With the diverging orbits of Fig. 5, however, we see trapping favoring the $\phi_{i_P^2} \approx 0°$ equilibrium point. Evidently the drag force and the strong earlier resonance combine to make the $\phi_{i_P^2} \approx 0°$ equilibrium point stable when it is normally unstable (Murray and Dermott, 1999); this unusual circumstance allows i_P to grow in a second-order resonance despite the diverging orbits.

We can qualitatively account for the effects of one resonance on another by extending Eq. (13) and the equivalent expression for $\ddot{\phi}_{i_P^2}$ to include both perturbations:

$$\ddot{\phi}_{e_P i_T^2} = -\omega_0^2 \sin\phi_{e_P i_T^2} - \omega_1^2 \sin\phi_{i_P^2} - \left(\dot{n}_G^d - 2\dot{n}_P^d\right), \tag{14}$$

$$\frac{\ddot{\phi}_{i_P^2}}{2} = -\omega_1^2 \sin\phi_{i_P^2} - \omega_0^2 \sin\phi_{e_P i_T^2} - \left(\dot{n}_G^d - 2\dot{n}_P^d\right), \tag{15}$$

with

$$\omega_1^2 = \frac{12\beta'(i_P^{\text{fr}})^2}{a_P^2}\left(2\mu_G + \sqrt[3]{2}\mu_P\right).$$

Here β', similar to β, is the resonant strength of $R_{i_P^2}$. Since $q = 2$ for the $R_{i_P^2}$ resonance, $\beta' > 0$. The libration of both $\phi_{e_P i_T^2}$ and $\phi_{i_P^2}$ are now modulated by new oscillations, and the presence of these new terms breaks both adiabatic invariants.

Equations (14) and (15) admit both oscillating and circulating solutions—ultimately the system is driven to the circulating solution. Which resonance is exited first depends on the relative resonant strengths and on the conditions when the second resonance is first encountered. In this example, the $R_{i_P^2}$ resonance is destroyed first, which allows the unperturbed $R_{e_P i_T^2}$ resonance to resume decreasing its libration amplitude in accordance with the adiabatic invariant.

The possibility of resonant capture complicates our study of the inclination history of the small satellites because of the difficulty in predicting inclination growths. While the two orbits are trapped into $R_{i_P^2}$, the free inclination of Proteus keeps growing. It is not obvious when the resonance will be broken, and hence it is difficult to estimate $i_P^{\rm fr}$ after traversal of the resonant zone. We find four cases amongst ∼200 simulations for different resonant zones, and the inclinations are affected only in one of these four cases. Since the capture probability is low, the limitation may not be serious. The actual capture probability might be higher than 2%, however, because our modeled $\frac{Q_N}{\bar{\rho}/(\mathrm{g/cm^3})}$ ranges from 1000 to 30,000. A smaller Q_N leads to artificially rapid orbital evolution which precludes some of the weak trapping events.

3.4. The chaotic PL 3:2

As we follow Proteus and Larissa backward in time to the *PL 3:2* resonant zone, the satellites are closer and the typical spacing between resonances is also smaller. When two strong resonances are very close together, their effective widths can overlap, causing the system to display chaotic behavior (see discussion in Zhang and Hamilton, 2007). During the *PL 3:2* resonance passage (Fig. 6), the semi-major axis of Larissa drops so much during the R_{e_L} resonance that R_{e_P} becomes important before the system escapes completely from the first resonance, resulting in temporary trapping into both resonances and chaotic changes to the orbits. While in the two first-order eccentricity-type resonances, random kicks to the semi-major axes bring a series of higher-order inclination-type resonances into and out of play, including the strong $R_{e_L i_P i_T}$ discussed in Zhang and Hamilton (2007). Chaotic kicks by these resonances, some of which are crossed multiple times, force the free inclinations of the two satellites to wander randomly. The width of the chaotic region depends on the resonant strengths, and hence the masses of the satellites. The tidal migration rate also plays a non-trivial role. Stronger resonances result in wider chaotic regions, and in turn, larger inclination growth. This imposes an immediate problem in estimating the inclination growth through the traverse of the *PL 3:2* resonant zone.

3.4.1. Eccentricity resonances overlapping criterion

It is important to be able to estimate when resonant overlapping occurs. Wisdom (1980) derived such a criterion for

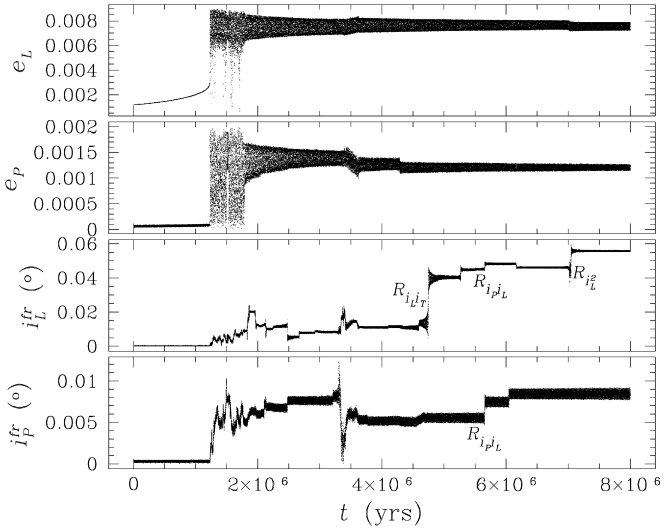

Fig. 6. The *PL 3:2* passage. The inclinations of the satellites follow a random walk behavior due to the chaotic overlap of the first-order eccentricity resonances. This interaction forces multiple crossings of weaker resonances that affect inclinations. Subsequent to escaping from the chaotic region, additional resonances are traversed. Several second-order resonances are indicated, while other strong ones are located in the chaotic zone and are not easily identified. The density of the satellites is $\bar{\rho} = 0.6$ g/cm^3 and $Q_N = 20{,}000$.

two first-order eccentricity resonances in two adjacent resonant zones, taking one satellite to be a test particle. For the neptunian satellites, resonant zones are well-separated for small p in Eq. (1). In the case of Proteus and Larissa, overlap of resonant zones requires $p \gtrsim 50$, i.e., beyond the *PL 51:50* zone, which only occurs when the satellites are extremely close together. For the vast majority of their evolution history, the two moons were separated enough that this type of overlap does not occur. Within a single resonant zone, however, resonant overlap is much more common as we have seen in Fig. 6. Here we determine the criterion under which the two first-order eccentricity resonances of a single resonant zone overlap; similar analyses are also possible for second-order eccentricity and inclination resonances. This type of overlap is particularly important when the two satellites have comparable masses.

The overlap condition is determined by comparing the resonance widths and the spacing between the two resonant centers. Murray and Dermott (1999) calculated the half-widths for the two first-order $p+1{:}p$ resonances in terms of the variation of the orbital semi-major axis of either Proteus or Larissa, which read

$$\left|\frac{(\Delta a)_{1/2}}{a}\right|_{e_L} = 4\left[-\frac{\alpha f_d(\alpha)\mu_P}{3} e_L^{\rm res}\right]^{1/2} \tag{16}$$

and

$$\left|\frac{(\Delta a)_{1/2}}{a}\right|_{e_P} = 4\left[-\frac{\alpha^3 f_d(\alpha)\mu_L}{3} e_P^{\rm res}\right]^{1/2} \tag{17}$$

for R_{e_L} and R_{e_P}, respectively. Here $\alpha = a_L/a_P = [p/(p+1)]^{2/3}$ is the semi-major axis ratio; $f_d(\alpha)$ is the coefficient for the first-order direct term in the expansion of the disturbing function; it is negative and its magnitude increases with α. The

values of $f_d(\alpha)$ for small p can be found in Table 8.5 of Murray and Dermott (1999), and we find that $\alpha f_d(\alpha) \approx -0.8p$ gives an excellent fit. The eccentricities of Larissa and Proteus when they are exactly in resonance are denoted by $e_L^{\rm res}$ and $e_P^{\rm res}$, respectively. When resonant kicks occur, however, $e_L^{\rm res}$ and $e_P^{\rm res}$ are not well defined since both eccentricities jump during the resonance. For example, in the *PL 2:1* zone (Fig. 3), $e_L \approx 0.003$ right before the R_{e_L} encounter, while $e_L \approx 0.011$ right afterward. Here we use the values right after the resonant crossings, given by Murray and Dermott (1999):

$$e_L^{\rm res} = 2\left[-\frac{\alpha f_d(\alpha)\mu_P}{3p^2}\right]^{1/3},$$

$$e_P^{\rm res} = 2\left[-\frac{\alpha^3 f_d(\alpha)\mu_L}{3p^2}\right]^{1/3}.$$

Note that this might over-estimate the resonant widths and bring in an error of about 50%. Using these eccentricities and the approximation $f_d(\alpha) = -0.8p$, we find

$$\left|\frac{(\Delta a)_{1/2}}{a}\right|_{e_L} = 2.34\sqrt[3]{\mu_P^2 p}, \tag{18}$$

$$\left|\frac{(\Delta a)_{1/2}}{a}\right|_{e_P} = 2.34\sqrt[3]{\mu_L^2 \alpha^4 p}. \tag{19}$$

These approximations show that resonances are stronger and wider for more closely spaced and more massive satellites.

Recall that $(\Delta a)_{1/2}/a$ can be the orbital size variation of either Proteus or Larissa in Eqs. (16)–(19) when the semi-major axis of the other planet is fixed. Assuming that a_L is fixed, we now calculate the separation between the two resonances in terms of a_P to compare with the resonance widths. Values of a_P for R_{e_L} and R_{e_P} in the same $p+1{:}p$ resonant zone can be obtained by setting the derivatives of the appropriate resonant arguments to zero:

$$\dot{\phi}_{e_L} = (p+1)n_P - pn_L - \dot{\tilde{\varpi}}_L = 0,$$

$$\dot{\phi}_{e_P} = (p+1)n_P - pn_L - \dot{\tilde{\varpi}}_P = 0.$$

The difference in a_P gives the spacing between the two resonances:

$$\frac{\delta a_P}{a_P} = \frac{2}{3}\frac{1}{p+1}\left(\frac{\dot{\tilde{\varpi}}_L - \dot{\tilde{\varpi}}_P}{n_P}\right) = J_2\left(\frac{R_N}{a_P}\right)^2 \frac{1-\alpha^{7/2}}{p\alpha^2}, \tag{20}$$

where we have assumed that the precession rates are dominated by planetary oblateness (Danby, 1988) and J_2 is the oblateness coefficient. The two eccentricity resonances are closer to each other for larger p, when the two orbits are closer to each other, and for slower orbital precession rates, when the satellites are further away from Neptune. Resonant separations are larger for satellites of Jupiter and Saturn than for those of Uranus and Neptune due to the differences in J_2 values. For $J_2 \approx 0$, as for the Sun, precession rates are dominated by secular effects and resonance overlap is more common.

Resonance overlap occurs when the sum of the two half-widths (Eqs. (18)–(19)) exceeds the separation (Eq. (20)):

$$2.34p\alpha^2\left(\sqrt[3]{\mu_P^2 p} + \sqrt[3]{\mu_L^2 \alpha^4 p}\right) \gtrsim J_2\left(\frac{R_N}{a_P}\right)^2 \left(1-\alpha^{7/2}\right). \tag{21}$$

Table 2
Critical resonances for first-order eccentricity resonance overlap

Satellite pair	Critical p	Critical resonance
PL	2	3:2
PG	2	3:2
PD	2	3:2
LG	5	6:5
LD	5	6:5
GD	6	7:6

Now we neglect the contribution from the R_{e_P} resonance in Eq. (21), which causes only an error of about 20% since $\mu_P \approx 10\mu_L$, and solve for large p:

$$p \gtrsim \left[\frac{J_2^3}{\mu_P^2}\left(\frac{R_N}{a_P}\right)^6\right]^{1/7}. \tag{22}$$

Although for most satellites the critical p is small, the assumption of large p only adds an error of about 50% even for $p = 1$. As with Wisdom (1980)'s overlap expression $p \gtrsim 0.51\mu^{-2/7}$, Eq. (22) also depends on $\mu^{-2/7}$. Assuming $\bar{\rho} = 0.6$ g/cm^3, resonance overlap occurs when $p \gtrsim 1.9$ for Proteus and Larissa (the exact solution of Eq. (21) gives $p \gtrsim 2.3$), which roughly agrees with our simulations: the *PL 3:2* ($p = 2$) has resonance overlap, while the *PL 2:1* ($p = 1$) does not.

We calculate the critical resonance where overlap first occurs for the four neptunian satellites in Table 2. Since the resonance widths are dominated by the larger mass, the three Proteus pairs have the same critical resonance. The two Larissa pairs also have the same critical resonance, but this time due to the similar sizes of Galatea and Despina.

This "collision" between eccentricity resonances and the resulting chaotic zone exists for all first-order resonances when the overlap criterion is met. During the *PL 3:2* passage shown in Fig. 6, for example, if the density of the satellites is less than 0.6 g/cm^3 and $Q_N < 20{,}000$, the system shows only very weak chaos; since the resonances barely overlap, significant growth of inclinations does not take place. If the satellites are more massive, or if they diverge more slowly, however, the random walk of the orbital elements can continue for a long time, the orbits become highly excited, and so the chaotic nature of this resonant zone wipes out all information from earlier times.

4. Discussion

4.1. Satellite densities

The magnitude of each resonant kick depends on the masses of the satellites, on their initial inclinations and eccentricities, and more weakly, on the tidal drag rate. As long as the two satellites diverge from each other so slowly that the major resonances are traversed in the adiabatic limit, however, the inclination growth is nearly independent of the migration rate. Since the four small satellites have probably migrated by less than a Neptune radius during their lifetime, our simulations show that most first- and second-order resonances are traversed adiabatically. Effects of higher-order resonances are usually in-

Table 3
Inclination kicks through different resonance passages (in degrees)

Resonance	Satellite	Density (g/cm^3)					
		1.5	1.2	1.0	0.8	0.6	0.4
PL 2:1	Proteus	0.026	0.022	0.018	0.017	0.014	0.012
	Larissa	0.1	0.095	0.090	0.085	0.070	0.057
PD 3:1	Proteus	0.0076	0.0065	0.0060	0.0058	0.0050	0.0040
	Despina	0.090	0.082	0.076	0.070	0.050	0.052
PG 2:1	Proteus	0.016	0.015	0.015	0.013	0.011	0.008
	Galatea	0.100	0.095	0.085	0.085	0.063	0.042
PL 5:3	Proteus	0.013	0.013	0.012	0.011	0.0095	0.0080
	Larissa	0.08	0.075	0.068	0.062	0.056	0.048

Pre-resonance free inclinations and eccentricities are set to zero in all of these simulations.

significant at these migration rates, but can occasionally lead to resonant trapping as discussed above.

In principle, with a system of resonances traversed in the adiabatic limit, we can derive the resonant kick magnitudes analytically to determine how the kicks depend on satellite masses, as is done for two-body resonances by Yoder (1973), Hamilton (1994), and Murray and Dermott (1999, Section 8). However, for the neptunian satellites, this derivation requires a Taylor expansion of the three-body disturbing function, which is beyond the scope of this work. Here we follow Zhang and Hamilton (2007) and take a numerical approach. We have done simulations for the individual resonant zones discussed in Section 3 with mean satellite density ranging between 0.4 and 1.5 g/cm^3, and satellite free inclinations and eccentricities initially set to zero. In Table 3 we summarize the overall inclination kicks on all satellite through the most recent four resonant zones. In Zhang and Hamilton (2007), we found that the overall inclination growth through the *PL 2:1* resonant zone was increased for larger satellite masses and densities. As might be expected, the same dependence holds true for other resonant zones as well, as shown in Table 3. Thus, we are able to derive the satellite masses by matching the total amount of inclination growth that a satellite obtains through multiple resonant passages to its current observed tilt. Two issues need to be resolved before we can compute the masses: (i) correcting for the effect of non-zero inclinations prior to resonant crossings, and (ii) determining which resonances have actually occurred.

For issue (i), we ran sets of simulations to measure the effects of the initial free inclinations on the magnitudes of kicks for the five strongest three-body resonances in the *PL 5:3* and *PL 2:1* resonant zones. We find that the initial free inclination of Proteus does not significantly affect the kicks on Larissa, and vice versa, confirming that the resonant kicks are mostly forced by Triton rather than the closer moon. Since the resonant strength is proportional to satellite inclinations, we might expect that larger initial tilts would result in stronger kicks. Surprisingly, however, the kick magnitude decreases extremely rapidly with increasing initial inclination of the affected satellite, as shown in Fig. 7. The simulation data from all individual three-body resonances is remarkably well fit by

$$\Delta i = \frac{\Delta i_0}{\sqrt{1+2\frac{i_0}{\Delta i_0}}}, \tag{23}$$

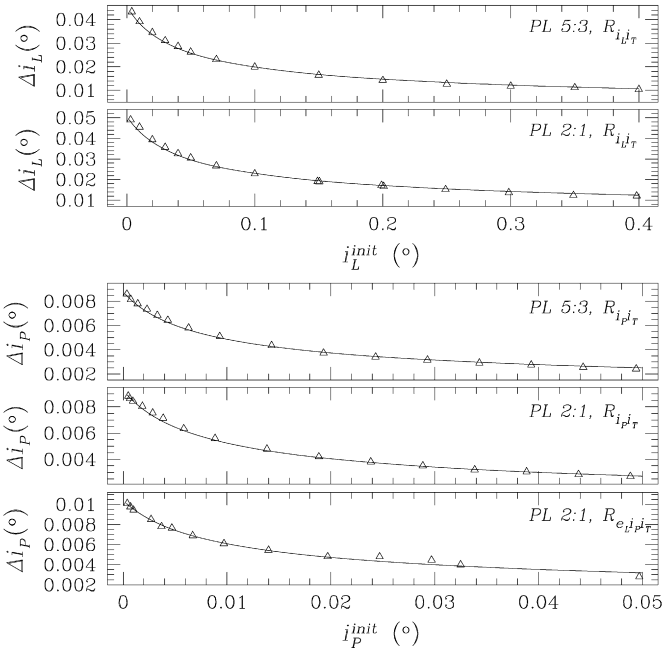

Fig. 7. Magnitudes of the three-body resonant kicks versus the satellites' initial free inclinations for five resonances. The top two panels show the $R_{i_L i_T}$ kicks on Larissa during *PL 5:3* and *PL 2:1* passages. The bottom three panels show the $R_{i_P i_T}$ and $R_{e_L i_P i_T}$ kicks on Proteus during the same passages. Triangle: kick magnitudes from different numerical simulations with various initial free inclinations; solid line: curves fit to Eq. (23).

where i_0 is the initial inclination, Δi is the kick magnitude, and Δi_0 is the kick magnitude at $i_0 = 0°$. We determine Δi_0 through the fitting process, finding excellent agreement with numerical simulations as seen in Fig. 7. If we treat the vertical oscillations as a simple harmonic oscillator, then Δi represents an amplitude change and the energy in the oscillation is proportional to i^2. The energy pumped into the system by each resonance is then

$$\Delta E \propto (i_0 + \Delta i)^2 - i_0^2 = \left[\frac{1 + 2i_0/\Delta i}{1 + 2i_0/\Delta i_0}\right]\Delta i_0^2.$$

The term in brackets is an increasing function of i_0 since $\Delta i_0 > \Delta i$ for all i_0. Thus, although the amplitude of the inclination kick decreases for increasing initial inclination i_0, the energy input actually increases.

Since kicks from these three-body resonances dominate the inclination growth and all obey the same equation, the overall change in inclination attained from passage through a full resonant zone follows approximately the same rule. A rough calculation leads to an error estimate of less than 10%. Equation (23) shows that the contribution to inclination growth by a resonant zone passage is more significant if the resonances occur earlier in time when the satellites' free inclinations are still small. For example, the *PL 2:1* passage can kick Larissa's inclination up to 0.085° ($\bar{\rho} = 0.8$ g/cm^3) if it is the only resonant zone the satellite has gone through, but if the satellite already has a 0.1° free tilt excited by earlier resonances, then the kick is only 0.046° according to Eq. (23).

Issue (ii) arises because we do not know the tidal evolution timescale. Fortunately, however, the current free inclinations of Proteus, Larissa, Galatea, and Despina provide strong constraints on the number of past resonant encounters. The observed free tilts of Galatea and Despina are both about 0.06°, Larissa's free inclination, at ∼0.2°, is three times as large, and Proteus has a smaller inclination of 0.026° (Table 1). Since the first three satellites have similar masses (within a factor of 2), we expect Galatea and Despina each to pass one strong resonant zone with Proteus (Fig. 2), and Larissa probably has passed more than one. Proteus is ∼10 times more massive than the other satellites, making it simultaneously the strongest perturber in the system and the hardest to perturb. For this reason, its free inclination is significant although it is the smallest among the four.

We now combine the results from Table 3, scaled by Eq. (23) as appropriate, and plot the final free inclinations acquired by the satellites for several possible past histories in Fig. 8. The curves for each satellite are represented by step functions with steps occurring at resonant zones that involve that satellite. It is important to realize that these curves are not evolution tracks, but are rather final status plots: inclinations at any given point in the past represent the predicted orbital tilts of the satellites today assuming that the system formed at that past time. We only calculate kicks for the most recent four Proteus resonances since the chaotic behavior of *PL 3:2* prevents any useful estimates of prior inclination growth. The curves for Galatea and Despina are very simple (with only one step) because they can each be involved in at most one major resonant zone passage. Larissa may go through two major zones, and there are four possible ones for Proteus.

If *PL 2:1* is the only resonant zone that the system has gone through, then Fig. 8 shows that, with a mean density of 1.5 g/cm^3, $i_P^{\rm fr}$ can be kicked up to near its current value, but Larissa can only obtain about half of today's orbital tilt. This agrees with our conclusion from Zhang and Hamilton (2007). If the system starts from an earlier configuration to include both the *PD 3:1* and the *PG 2:1* resonant zones, the inclinations of both Galatea and Despina can be pushed high enough with a density satisfying $0.4 < \bar{\rho} < 0.8$ g/cm^3. For $i_P^{\rm fr}$ to reach 0.026° in this case, however, a density of $0.6 < \bar{\rho} < 1.0$ g/cm^3 is required. With an earlier formation time so that all four Proteus resonances are traversed, however, the density required by Proteus's free inclination also drops to $0.4 < \bar{\rho} < 0.8$ g/cm^3 due to the extra kick from Larissa.

Densities as low as $0.4 < \bar{\rho} < 0.8$ g/cm^3 imply large porosities, but similar values are measured for both saturnian and jovian satellites. Nicholson et al. (1992) determined the densities of Saturn's co-orbital satellites, Janus and Epimetheus, at $\bar{\rho} \approx 0.6$ g/cm^3. More recently, Renner et al. (2005) measured the densities of Prometheus (0.4 g/cm^3) and Pandora (0.49 g/cm^3); Porco et al. (2005) also estimated the densities of Atlas and Pan to be ∼0.5 g/cm^3. All these saturnian satellites are made of nearly-pure porous water ice. The density of the jovian satellite Amalthea ($\bar{\rho} = 0.9$ g/cm^3, Anderson et al., 2005) is a little bit higher, but the satellite is made of a mixture of water ice and rock, and high porosity is also expected. Thus our density determination is physically plausible.

4.2. Larissa's story

Three or four Proteus past resonance passages provide a consistent solution for the free tilts of Proteus, Galatea, and Despina with $0.4 < \bar{\rho} < 0.8$ g/cm^3, a density range that is physically plausible. But the current inclination of Larissa cannot be matched with the assumptions of equal satellite densities in any of the scenarios considered so far. Even if all four Proteus resonance zones were traversed, Larissa could attain just over one half its current inclination for this density range. In fact, $i_L^{\rm fr}$ can only be excited to ∼0.14° even if the mean density is as high as 1.5 g/cm^3. What happened to Larissa?

The first potential solution to explaining Larissa's large tilt is to allow satellites to have different densities. But this leads immediately to the same problem that we faced in Zhang and Hamilton (2007): in order for $i_L^{\rm fr}$ to be kicked more, we need a more massive Proteus, or a less massive Larissa. The mass of Proteus cannot be increased much since this would result in larger inclinations for Galatea and Despina than currently observed (Fig. 8). Reducing Larissa's mass helps a little, but the dependence of the *PL* kick strengths on Larissa's mass is very weak since Proteus is the dominate mass. Our simulations show that the cumulative inclination kick on Larissa only increases from 0.1° to ∼0.13° if we drop ρ_L from 0.6 to 0.05 g/cm^3 while keeping ρ_P at 0.6 g/cm^3. Even this unrealistically-low satellite density does not solve the problem.

A second possible solution is to allow Larissa to pass through more resonances. The next Proteus–Larissa resonant zone is the chaotic *PL 3:2*. For this zone, our simulations indicate that chaotic behavior becomes significant only for density $\bar{\rho} > 0.8$ g/cm^3, in which case Proteus usually gets an overall kick >0.025° through the random walk process. Adding kicks from later resonances, this results in too large a tilt. However, for density $\bar{\rho} \leqslant 0.6$ g/cm^3, the chaotic behavior is weak and the orbital inclination growths are reasonable. In our example shown in Fig. 6 ($\bar{\rho} = 0.6$ g/cm^3), the kicks on Proteus and Larissa are 0.009° and 0.06°, respectively, which bring the overall inclination growths of the two satellites through the 5 resonance passages to $i_P^{\rm fr} = 0.029°$ and $i_L^{\rm fr} = 0.128°$, where we have used Eq. (23) to model the later kicks. If $\bar{\rho} = 0.4$ g/cm^3, the *PL 3:2* kicks on the two satellites are 0.008° and 0.05°,

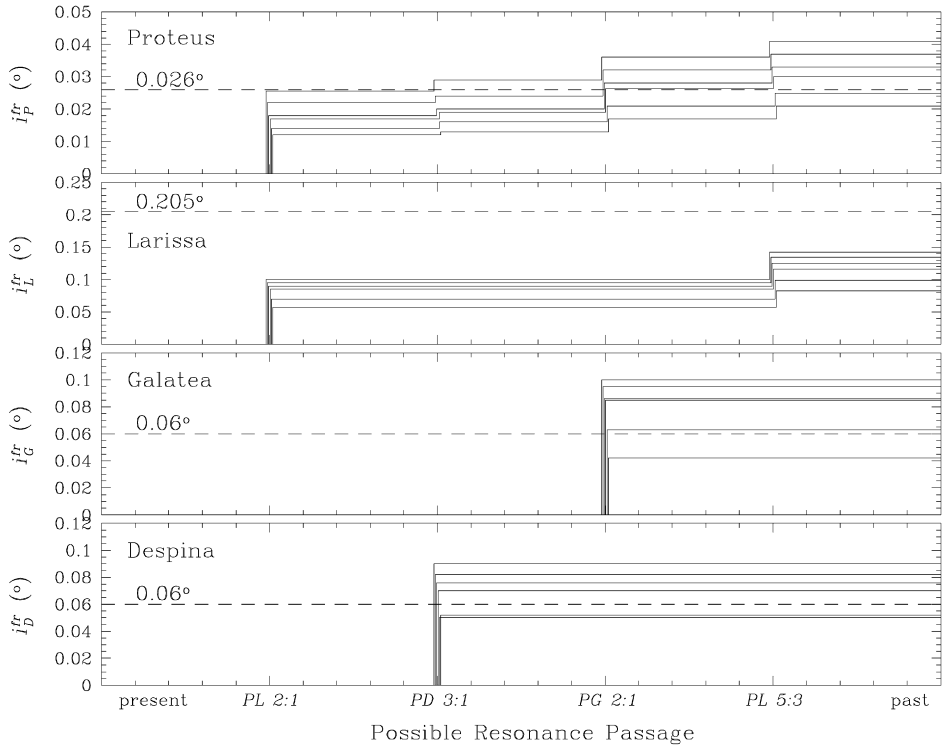

Fig. 8. The cumulative free inclinations of Proteus ($i_P^{\rm fr}$), Larissa ($i_L^{\rm fr}$), Galatea ($i_G^{\rm fr}$), and Despina ($i_D^{\rm fr}$). The curves show the final free inclinations that the satellites acquire versus their formation time represented in terms of resonant zone passages (cf. Fig. 2). Resonances to the left of the formation time have actually occurred, while those to the right have not. We assume all satellites have the same bulk densities; solid curves represents different densities: from top to bottom: $\bar{\rho} = 1.5, 1.2, 1.0, 0.8, 0.6, 0.4$ g/cm^3. The single exception to this is the Despina 0.4 curve which is actually above the 0.6 curve due to stochastic variations. The dashed horizontal lines represent the current free inclinations of the satellites.

which can only promote the inclination growth of Larissa to a total of $i_L^{\rm fr} = 0.107°$. Although the actual inclination kicks may vary, our simulations show that for a specific density, they all fall in the same range. Hence, Larissa's orbit cannot be effectively tilted even if this troublesome resonant zone is included. Perhaps there is a rare outcome of the chaotic interactions in which Larissa's inclination is highly excited, but we have seen no evidence that this is the case. Including earlier resonances is problematic: the preceding one, *PD 2:1*, excites the inclination of Despina, forcing Proteus' density to $\bar{\rho} < 0.4$ g/cm^2 to keep that satellite's inclination low and making it less likely to produce similar tilts for Despina and Galatea. The earlier *PG 5:3* would then be required. The trend here is clear—additional *PD* and *PG* resonances force Proteus' density down, making additional *PL* resonances less effective. Tweaking the tidal model might change the order of some resonances (e.g., the *PL 3:2* and *PD 2:1*), but our basic conclusion is unaltered. There is no set of Proteus resonances that can simultaneously make the inclination of Larissa large while keeping those of Galatea and Despina low.

A third possibility includes invoking the weaker, but more numerous, resonances among the three smaller satellites (Fig. 2), which we have neglected until now. Could the inclusion of these resonances solve the problem of Larissa's inclination excess? Since the masses of Larissa, Galatea, and Despina are 10 times smaller than Proteus', these resonances are very weak even though the satellites are closer to one another than to Proteus. Our simulations show that typically inclinations of both satellites obtain a $\sim 0.01°$ overall growth through a single zone passage, assuming zero initial free inclinations. The cumulative effect of these kicks could potentially be large given that there are so many of them. However, due to the strong dependence of the kick magnitude on the initial free inclinations, these weak kicks, albeit numerous, do not add much to the satellite's free tilts, especially for the ones occurring after any of the more powerful Proteus resonances. Furthermore, Fig. 2 shows that Larissa, Galatea, and Despina all have traversed a similar number of these weak resonant zones—in fact, Galatea receives more kicks than the other two because of its central location. Thus it is nearly impossible to increase Larissa's inclination significantly while keeping those of the other two moons small. Inclusion of these resonances, however, does systematically drive our solution for $\bar{\rho}$ towards slightly lower values.

A fourth possible cause of Larissa's inclination excess is that the satellite might actually have been captured into a resonance. We have seen an unusual inclination capture following a three-body eccentricity capture with the result that both Proteus' eccentricity and inclination are forced to increase (Fig. 5). Although the chance is low, it is possible that Larissa was once captured into a similar resonance ($R_{i_L^2}$) with either Galatea or Despina. Fig. 2 shows that there are several possibilities, with earlier resonances more likely to capture Larissa than later ones because its inclination was smaller in the past. Expanding our

search to include the tiny inner moons, Naiad and Thalassa, we note that captures are more likely since Larissa's orbit is approaching the inner two orbits and trapping into strong low-order inclination resonances is possible. Naiad's extremely high free inclination also points to a previous capture (Banfield and Murray, 1992), and Larissa would be a natural candidate. Assuming that Larissa's semi-major axis migrated from the synchronous orbit to its current orbit, Larissa's interior 2:1 resonance would move from $2.08R_N$ to $1.83R_N$, which brackets the current orbit of Naiad at $1.91R_N$. Although Naiad was somewhat further away from Neptune in the past, there is a good chance that the 2:1 Larissa–Naiad resonance did actually occur. Similarly, Larissa's 2:1 or 5:3 internal resonances may have swept across Thalassa's orbit, implying possible strong interactions with that satellite. The odds of capture into a resonance involving Larissa's inclination is a strong decreasing function of its initial tilt, and it is hardly possible if Larissa's orbit is inclined by more than some critical value (Borderies and Goldreich, 1984). Hence, the capture probably occurred earlier on. Two main possibilities exist: (i) capture occurred prior to the *PL 5:3*, with two subsequent Larissa kicks from the *PL 5:3* and *PL 2:1*, and (ii) the *PL 5:3* never occurred and there was only one Larissa kick (*PL 2:1*) after the capture. For the density range $0.4 < \bar{\rho} < 0.8$ g/cm^3, scenario (i) requires Larissa to have a free inclination of 0.14° after escaping from the hypothetical resonant capture, while in scenario (ii), the satellite needs to have a 0.16° free tilt after escape. Although requiring an additional resonant capture, we think that this is the most likely scenario and will pursue the details in a future publication.

4.3. Tidal evolution timescale and Q_N

The four satellites have most likely passed though three or four strong Proteus resonant zones: definitely the *PL 2:1*, the *PD 3:1*, and the *PG 2:1*, and possibly the *PL 5:3* before those. If the system formed with a configuration between *PL 3:2* and *PG 2:1* in Fig. 2, this provides a natural explanation for the inclinations of at least three of the four satellites. We enlarge this region of the plot in Fig. 9. Due to the observational error in satellite size measurements (Table 1), which leads to mass uncertainties, the evolution tracks of Proteus and Larissa fall somewhere within the lightly-shaded area in Fig. 9, resulting in uncertainties in the locations of *PL 3:2* ($4.99 < t < 6.06$ Gyr) and *PG 2:1* ($2.92 < t < 3.72$ Gyr), as indicated by the darkly-shaded area. As discussed before, the evolution timescale is affected by Q_N and $\bar{\rho}$. Thus, we estimate that the system formed at

$$\left(\frac{Q_N/20{,}000}{\bar{\rho}/(0.6\ \mathrm{g/cm^3})} \times 2.92\ \mathrm{Gyrs}\right) < t < \left(\frac{Q_N/20{,}000}{\bar{\rho}/(0.6\ \mathrm{g/cm^3})} \times 6.06\ \mathrm{Gyrs}\right). \quad (24)$$

Triton was most likely captured at a very early stage of Solar System history (~4.5 Gyr ago), when there were still plenty of planetesimals for Neptune to interact with. The circularization of Triton takes merely a few 100 Myr, thus we assume that the inner satellites date back to ~4 billion years. Substituting $t \approx 4$ Gyrs and $0.4 < \bar{\rho} < 0.8$ g/cm^3 into Eq. (24), we estimate

$$9000 < Q_N < 36{,}000.$$

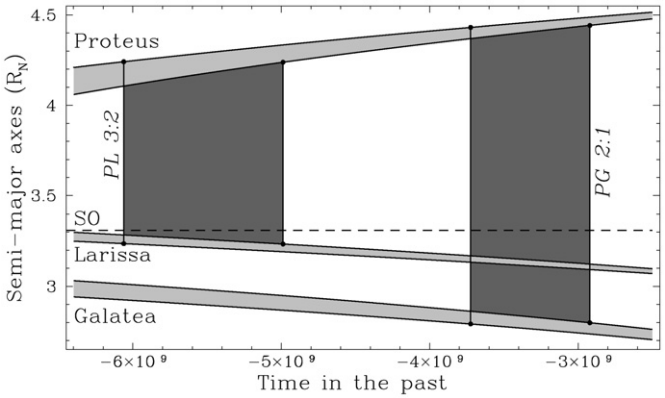

Fig. 9. Possible initial configurations of the system. The plot shows a magnified region of Fig. 2. The evolution tracks of Proteus, Larissa, and Galatea lie anywhere in the respective lightly-shaded areas. The darkly-shaded areas show the possible locations of *PL 3:2* and *PG 2:1* resonant zones. The boundaries of these areas are determined by the observational uncertainties of satellite sizes. The system started with an initial configuration between the earliest possible *PL 3:2* and the latest possible *PG 2:1*. As with Fig. 2, times need to be multiplied by the factor $\frac{Q_N/20{,}000}{\bar{\rho}/(0.6\ \mathrm{g/cm^3})}$.

Part of this uncertainty comes from satellite size and density uncertainties, while the rest comes from not knowing whether the system formed closer to *PL 3:2* or *PG 2:1*. Although 4 Gyrs is a feasible age for the small satellites, they may have been subsequently destroyed by cometary bombardment as suggested by Smith et al. (1989). This effectively resets the clock to the time of destruction and lowers both bounds on Q_N. Nevertheless, we believe that this late and complete destruction of the inner neptunian satellites is not a very likely possibility. Another uncertain factor that affects the Q_N determination is k_{2N}. The Love numbers of giant planets are computed by several authors with different models. We have adopted $k_{2N} = 0.41$ from Burša (1992), while an earlier estimation by Gavrilov and Zharkov (1977) gives a much smaller value ($k_{2N} = 0.13$). Since the tidal constraints are actually on Q_N/k_{2N} (Eq. (2)), the smaller Love number would lead to a drop in both the upper and lower bounds of Q_N by a factor of 3.

Banfield and Murray (1992) estimated Q_N with similar method but different dynamical constraints. They took $k_{2N} = 0.39$ based on a model by Dermott et al. (1988), assumed satellite densities to be ~1.2 g/cm^3, and obtained a lower limit $Q_N > 12{,}000$ by requiring Proteus to form outside of the synchronous orbit and an upper limit $Q_N < 330{,}000$ from the Naiad capture event. As our determined satellite density of 0.4–0.8 g/cm^3 is half that assumed by Banfield and Murray (1992), we scale their Q_N estimates to $4000 < Q_N < 220{,}000$ so that they can be directly compared to our estimates. Instead of assuming that Proteus migrated from the synchronous orbit ($3.31R_N$), we have shown that the satellite could not have formed closer than $4.20R_N$ in order to avoid the *PL 3:2* resonance. This explains the factor of 2 difference between our lower bound of $Q_N > 9000$ and that of Banfield and Murray

Table 4
Q of giant planets

Planet	Author	Q	k_2	Q/k_2
Jupiter	GS66	$\geqslant$100,000	1.5	$\geqslant$66,000
	YP81	$(0.6–20) \times 10^5$	0.379 (GZ77)	1.6×10^5–5×10^6
Saturn	GS66	$\geqslant$60,000	1.5	$\geqslant$40,000
	P80	$\geqslant$16,000	0.341 (GZ77)	$\geqslant$45,000
Uranus	GS66	$\geqslant$72,000	1.5	$\geqslant$48,000
	TW89	11,000–39,000	0.104 (GZ77)	105,000–375,000
Neptune	BM92	4000–220,000[a]	0.39 (D88)	10,000–560,000[a]
	This work	9000–36,000	0.41 (B92)	22,000–90,000

GS66: Goldreich and Soter (1966); GZ77: Gavrilov and Zharkov (1977); P80: Peale et al. (1980); YP81: Yoder and Peale (1981); D88: Dermott et al. (1988); TW89: Tittemore and Wisdom (1989); BM92: Banfield and Murray (1992); B92: Burša (1992).

[a] Values have been scaled with our determined satellite densities. The original limits given in Banfield and Murray (1992) are $12{,}000 < Q_N < 330{,}000$, assuming $\bar{\rho} = 1.2$ g/cm^3. The spread in their upper and lower limits would increase by a factor of 2 if satellite density uncertainties were included.

(1992). Our biggest improvement, a factor of 6 times reduction in the upper limit of Q_N, arises from the constraint that Proteus traversed at least 3 resonances.

Several authors have previously estimated Q for other giant planets based on similar dynamical constraints; we collect these results in Table 4 and compare them to our own. It is best to compare the values of Q/k_2 in the final column because this is the quantity directly constrained by all dynamical studies. Goldreich and Soter (1966) were the first to systematically investigate the planetary Q's in the Solar System. Based on the known satellites at that time, they estimated lower limits of Q for Jupiter ($Q_J \geqslant 100{,}000$), Saturn ($Q_S \geqslant 60{,}000$), and Uranus ($Q_U \geqslant 72{,}000$). They ignored the internal structure of the planets and assumed a uniform $k_2 = 1.5$. They also assumed that these satellites could initially migrate from the surface of the planet. The existence of synchronous orbits, however, reduces the amount of tidal migration and lifts these lower limits by a factor of 2–3. Yoder and Peale (1981) addressed this and obtained an improved lower bound for Jupiter's Q: $Q_J \geqslant 64{,}000$, using $k_{2J} = 0.379$ computed by Gavrilov and Zharkov (1977). Yoder and Peale (1981) also estimated the upper limit of Q_J based on tidal heating required by Io, and obtained $Q_J \leqslant 2 \times 10^6$. Peale et al. (1980) corrected Saturn's Q with more reliable k_{2S} from Gavrilov and Zharkov (1977), and estimated the lower bound to be $Q_S \geqslant 16{,}000$. The lower bounds of both Q_J/k_{2J} and Q_S/k_{2S} are larger than what we find for Neptune. Recall that Q is an empirical measurement of the energy dissipation properties of planets that is not well understood physically.

For Uranus, the closest sibling of Neptune, Tittemore and Wisdom (1989) placed Q_U between 11,000 and 39,000 based on the resonant history of the uranian satellites. However, their Q_U/k_{2U} value is about 4 times larger than our Q_N/k_{2N}. One might expect these two similar-sized planets to have similar Q and k_2. One possible explanation for the difference in Q/k_2 is different internal structures of the planets—Neptune is denser and radiates more of its internal heat.

4.4. Q_P and Q_L

The current eccentricities of Proteus and Larissa have significant non-zero values (Table 1), which we interpreted in Zhang and Hamilton (2007) as a signature of the recent *PL 2:1* resonance passage. Since satellite eccentricities damp away rapidly due to satellite tides with a time scale that depends on Q_S, while the timescale of satellite migrations due to planetary tides depends on Q_N, we can calculate the ratio Q_S/Q_N for Proteus and Larissa based on their tidal migration and eccentricity changes after the *PL 2:1* resonant encounter. In Zhang and Hamilton (2007), we derived

$$\frac{Q_S}{Q_N} = 7.5 \times 10^{-3} \times \left(\frac{R_s}{\text{km}}\right)\left(\frac{\text{g/cm}^3}{\bar{\rho}}\right)\left|\frac{\ln(a_f/a_i)}{\ln(e_f/e_i)}\right|. \tag{25}$$

Here R_s is the satellite radius in kilometers and a_i, a_f and e_i, e_f are the initial and final semi-major axes and eccentricities, respectively. We found that both Q_P and Q_L had a lower limit of 10 based on the density constraint from *PL 2:1* passage. As a result of our current work with much better constraints for satellite density and Q_N, we can improve our estimates of Q_P and Q_L.

With density between 0.4 and 0.8 g/cm^3, Proteus and Larissa can attain eccentricities of 0.0011–0.0014 and 0.008–0.01 during the *PL 2:1* passage, respectively. Since the location of *PL 2:1* is only affected by the mass ratio of the two satellites which determine their relative migration rate, we use the same migration distances as in Zhang and Hamilton (2007): 0.010–$0.013 R_N$ outward for Proteus and 0.014–$0.016 R_N$ inward for Larissa. Substituting these measurements into Eq. (25), we find

$$0.004 < \frac{Q_P}{Q_N} < 0.02, \qquad 0.002 < \frac{Q_L}{Q_N} < 0.006.$$

For $9000 < Q_N < 36{,}000$, this implies

$$36 < Q_P < 700, \qquad 18 < Q_L < 200.$$

This is an interesting result since the tidal Q of satellites is more poorly known than planetary Q's—very few dynamical events can provide useful constraints. The only satellite with a well-determined Q is our own Moon, with $Q_M = 27$ (Yoder and Ahrens, 1995). This is within the range of our estimates for Proteus and Larissa, but the size of the Moon is much larger than the two neptunian satellites. For other satellites of the giant planets, Goldreich and Soter (1966) estimated that $Q_S < 500$ based on a rough assumption of satellite rigidity. Yoder and Peale (1981) estimated Europa's Q with an eccentricity damping method similar to what we have used, and obtained $Q_E \gtrsim 2 \times 10^{-4} Q_J \approx 20$. They were also able to estimate Io's Q through an analysis of tidal heating of the melting moon: $Q_I \approx 0.001 Q_J \approx 100$. These values fall into the same general range as our estimates for Proteus and Larissa.

5. Conclusion

In this continued investigation of the resonant history of the inner neptunian satellites, we have examined the possible

mean-motion resonances between Proteus, Triton, and each of Larissa, Galatea, and Despina. The current free inclinations of these satellites are consistent with the magnitudes of the resonant kicks. Three past Proteus resonance passages, the *PL 2:1*, *PD 3:1*, *PG 2:1*, and possibly a fourth *PL 5:3*, can explain how the orbital tilts of Proteus, Galatea, and Despina were excited to their current valuers from $i < 0.001°$. The required satellite densities in this scenario are $0.4 < \bar{\rho} < 0.8$ g/cm^3, and are in line with low densities measured for the small saturnian and jovian satellites. These resonances, however, are too weak to excite Larissa's inclination from near zero to its current value, and an additional process is required. An earlier resonant trapping event is the most promising candidate, with Naiad or Thalassa resonances especially favored.

The requirement of the three or four Proteus resonance encounters, but none of the earlier ones (cf. Fig. 2), strongly constrains satellite semi-major axes at formation. Proteus' initial semi-major axis is restricted to 4.2–4.5R_N, which implies that the debris disk out of which these small satellites formed was about the same size. This provides a lower limit on the pericenter distance of Triton's post-captured orbit, restricting how deep inside the Neptune system Triton could have penetrated during its tidal circularization.

With our new limits on satellite densities, we find $9000 < Q_N < 36{,}000$, where we have assumed that the satellites formed 4 billion years ago. Our refined determination of $\bar{\rho}$ and Q_N enable us to derive better constraints on the satellite Q's; we find that Q_P is between 36 and 700, and Q_L between 18 and 200.

Acknowledgments

We are grateful to J.A. Burns and R. Greenberg for helpful discussions and valuable suggestions. We also thank the two reviewers for their careful and critical readings of our manuscript. This material is based upon work supported by the National Aeronautics and Space Administration under Grant No. NAG513100 issued though the Office of Space Science.

References

Agnor, C.B., Hamilton, D.P., 2006. Neptune's capture of its moon Triton in a binary-planet gravitational encounter. Nature 441, 192–194.

Anderson, J.D., Johnson, T.V., Schubert, G., Asmar, S., Jacobson, R.A., Johnston, D., Lau, E.L., Lewis, G., Moore, W.B., Taylor, A., Thomas, P.C., Weinwurm, G., 2005. Amalthea's density is less than that of water. Science 308, 1291–1293.

Banfield, D., Murray, N., 1992. A dynamical history of the inner neptunian satellites. Icarus 99, 390–401.

Borderies, N., Goldreich, P., 1984. A simple derivation of capture probabilities for the J + 1:J and J + 2:J orbit–orbit resonance problems. Celest. Mech. 32, 127–136.

Burns, J.A., 1977. Orbital evolution. In: Burns, J.A. (Ed.), Planetary Satellites. Univ. of Arizona Press, Tuscon, AZ, pp. 113–156.

Burša, M., 1992. Secular Love numbers of the major planets. Earth Moon Planets 59, 239–244.

Colombo, G., 1966. Cassini's second and third laws. Astron. J. 71, 891–896.

Ćuk, M., Gladman, B.J., 2005. Constraints on the orbital evolution of Triton. Astrophys. J. 626, L113–L116.

Danby, J.M.A., 1988. Fundamentals of Celestial Mechanics, second ed. Willmann–Bell, Richmond, VA.

Dermott, S.F., Malhotra, R., Murray, C.D., 1988. Dynamics of the uranian and saturnian satellite systems—A chaotic route to melting Miranda? Icarus 76, 295–334.

Gavrilov, S.V., Zharkov, V.N., 1977. Love numbers of the giant planets. Icarus 32, 443–449.

Goldreich, R., 1963. On the eccentricity of satellite orbits in the Solar System. Mon. Not. R. Astron. Soc. 126, 257–268.

Goldreich, P., Soter, S., 1966. Q in the Solar System. Icarus 5, 375–389.

Goldreich, P., Murray, N., Longaretti, P.Y., Banfield, D., 1989. Neptune's story. Science 245, 500–504.

Greenberg, R., 1973. Evolution of satellite resonances by tidal dissipation. Astron. J. 78, 338–346.

Greenberg, R., 1977. Orbit–orbit resonances among natural satellites. In: Burns, J.A. (Ed.), Planetary Satellites. Univ. of Arizona Press, Tuscon, AZ, pp. 157–168.

Hamilton, D.P., 1994. A comparison of Lorentz, planetary gravitational, and satellite gravitational resonances. Icarus 109, 221–240.

Hamilton, D.P., Burns, J.A., 1993. Lorentz and gravitational resonances on circumplanetary particles. Adv. Space Res. 13 (10), 241–248.

Hamilton, D.P., Ward, W.R., 2004. Tilting Saturn. II. Numerical model. Astron. J. 128, 2510–2517.

Hamilton, D.P., Zhang, K., Agnor, C., 2005. Tilting Saturn. II. Numerical model. Bull. Am. Astron. Soc. 37, 529.

Jacobson, R.A., Owen, W.M., 2004. The orbits of the inner neptunian satellites from Voyager, Earth-based, and Hubble Space Telescope observations. Astron. J. 128, 1412–1417.

Jacobson, R.A., Riedel, J.E., Taylor, A.H., 1991. The orbits of Triton and Nereid from spacecraft and Earth-based observations. Astron. Astrophys. 247, 565–575.

Karkoschka, E., 2003. Sizes, shapes, and albedos of the inner satellites of Neptune. Icarus 162, 400–407.

Landau, L.D., Lifshitz, E.M., 1976. Course of Theoretical Physics, vol. 1, third ed. Pergamon, Elmsford, NY.

McCord, T.B., 1966. Dynamical evolution of the neptunian system. Astron. J. 71, 585–590.

McKinnon, W.B., 1984. On the origin of Triton and Pluto. Nature 311, 355–358.

Murray, C.D., Dermott, S.F., 1999. Solar System Dynamics. Cambridge Univ. Press, Cambridge, UK.

Nicholson, P.D., Hamilton, D.P., Matthews, K., Yoder, C.F., 1992. New observations of Saturn's coorbital satellites. Icarus 100, 464–484.

Peale, S.J., 1976. Orbital resonances in the Solar System. Annu. Rev. Astron. Astrophys. 14, 215–246.

Peale, S.J., Cassen, P., Reynolds, R.T., 1980. Tidal dissipation, orbital evolution, and the nature of Saturn's inner satellites. Icarus 43, 65–72.

Porco, C.C., Baker, E., Barbara, J., Beurle, K., Brahic, A., Burns, J.A., Charnoz, S., Cooper, N., Dawson, D.D., Del Genio, A.D., Denk, T., Dones, L., Dyudina, U., Evans, M.W., Giese, B., Grazier, K., Helfenstein, P., Ingersoll, A.P., Jacobson, R.A., Johnson, T.V., McEwen, A., Murray, C.D., Neukum, G., Owen, W.M., Perry, J., Roatsch, T., Spitale, J., Squyres, S., Thomas, P., Tiscareno, M., Turtle, E., Vasavada, A.R., Veverka, J., Wagner, R., West, R., 2005. Cassini imaging science: Initial results on Saturn's rings and small satellites. Science 307, 1226–1236.

Renner, S., Sicardy, B., French, R.G., 2005. Prometheus and Pandora: Masses and orbital positions during the Cassini tour. Icarus 174, 230–240.

Smith, B.A., Soderblom, L.A., Banfield, D., Barnet, C., Basilevsky, A.T., Beebe, R.F., Bollinger, K., Boyce, J.M., Brahic, A., Briggs, G.A., Brown, R.H., Chyba, C., Collins, S.A., Colvin, T., Cook, A.F., Crisp, D., Croft, S.K., Cruikshank, D., Cuzzi, J.N., Danielson, G.E., Davies, M.E., De Jong, E., Dones, L., Godfrey, D., Goguen, J., Grenier, I., Haemmerle, V.R., Hammel, H., Hansen, C.J., Helfenstein, C.P., Howell, C., Hunt, G.E., Ingersoll, A.P., Johnson, T.V., Kargel, J., Kirk, R., Kuehn, D.I., Limaye, S., Masursky, H., McEwen, A., Morrison, D., Owen, T., Owen, W., Pollack, J.B., Porco, C.C., Rages, K., Rogers, P., Rudy, D., Sagan, C., Schwartz, J., Shoemaker, E.M., Showalter, M., Sicardy, B., Simonelli, D., Spencer, J., Sromovsky, L.A., Stoker, C., Strom, R.G., Suomi, V.E., Synott, S.P., Terrile, R.J., Thomas, P., Thompson, W.R., Verbiscer, A., Veverka, J., 1989. Voyager 2 at Neptune—Imaging science results. Science 246, 1422–1449.

Tittemore, W.C., Wisdom, J., 1989. Tidal evolution of the uranian satellites. II. An explanation of the anomalously high orbital inclination of Miranda. Icarus 78, 63–89.

Ward, W.R., Hamilton, D.P., 2004. Tilting Saturn. I. Analytic model. Astron. J. 128, 2501–2509.

Wisdom, J., 1980. The resonance overlap criterion and the onset of stochastic behavior in the restricted three-body problem. Astron. J. 85, 1122–1133.

Yoder, C.F., 1973. On the establishment and evolution of orbit–orbit resonances. Ph.D. thesis.

Yoder, C.F., 1995. Astrometric and geodetic properties of Earth and the Solar System. In: Ahrens, T. (Ed.), Global Earth Physics: A Handbook of Physical Constants. American Geophysical Union, Washington, pp. 1–31.

Yoder, C.F., Peale, S.J., 1981. The tides of Io. Icarus 47, 1–35.

Zhang, K., Hamilton, D.P., 2007. Orbital resonances in the inner neptunian system. Icarus 188, 386–399.